Hall2De Simulations with a First-principles Electron Transport Model Based on the Electron Cyclotron Drift Instability

Ioannis G. Mikellides,* Alejandro Lopez Ortega,† Ira Katz,‡ and Benjamin A. Jorns§
Jet Propulsion Laboratory, California Institute of Technology, Pasadena, CA, 91109

Abstract: Several years of work have combined plasma measurements in a laboratory Hall thruster and r-z numerical simulations with Hall2De to isolate the spatial variation of the anomalous collision frequency needed in Ohm's law to produce the observed thruster behavior. This numerical solution is used here to test the validity of a first-principles model of the anomalous transport in these devices before such model is implemented self-consistently in r-z fluid codes like Hall2De. The first-principles model employs quasi-linear theory and is based on the hypothesis that the Electron Cyclotron Drift Instability (ECDI) excites ion acoustic turbulence that, in turn, enhances the effective collision frequency in these devices. We find that a model of the ECDI that assumes Maxwellian velocity distributions for electrons and singly-charged, main-beam, cold ions (T_i=0.07 eV) is insufficient to explain the expected variation of the anomalous collision frequency both in the interior and exterior of the acceleration channel. When warm ions (~0.5-3 eV) are accounted for, the ECDI model in the channel interior appears more promising but fails by orders of magnitude in the near plume region due to the much higher Landau damping of the ion acoustic waves there. This implies that either (a) some process allows the ECDI instability to remain uninhibited by classical Landau damping or, (b) that a different instability (or instabilities) altogether, also insusceptible to Landau damping, is/are active in this region. A previous hypothesis, that convection of wave energy generated by the ECDI in the channel plays a significant role in the near plume, is not supported by the results of the simulations.

Hall thrusters on NASA deep-space science missions typically have lifetime requirements that far exceed those for near-Earth applications. For example, the Solar Electric Propulsion (SEP) system on the Asteroid Redirect Robotic Mission (ARRM) is required to operate for 30,000 hours.[1] ARRM is the leading candidate for a NASA SEP Technology Demonstration Mission planned for launch by the end the decade.[2-5] The ARRM thruster called Hall-effect Rocket with Magnetic Shielding (HERMeS) is a 12.5-kW Hall thruster that has been developed over the last few years by the NASA Glenn Research Center and the Jet Propulsion Laboratory to deliver system efficiency ≥57%, specific impulse up to 3000 s and propellant throughput of 3400 kg. Demonstration of such high throughputs cannot be performed by test alone due to time and cost limitations associated with vacuum facilities. Therefore, some combination of wear tests and physics-based numerical simulation must be utilized.

Anomalous transport of electrons across magnetic field lines is known to occur in Hall-effect thrusters but the physics that drive it have remained elusive for decades. Many theories have been proposed through the years but *ab initio* predictive numerical simulations of the plasma that span the acceleration

* Principal Engineer, Electric Propulsion Group, 4800 Oak Grove Drive, Pasadena, CA, 91109, Mail Stop 125-109, Associate Fellow AIAA.
† Member of the Technical Staff, Electric Propulsion Group, 4800 Oak Grove Drive, Pasadena, CA, 91109, Mail Stop 125-109, Member AIAA.
‡ Group Supervisor, Electric Propulsion Group, 4800 Oak Grove Drive, Pasadena, CA, 91109, Mail Stop 125-109, Senior Member AIAA.
§ Member of the Technical Staff, Electric Propulsion Group, 4800 Oak Grove Drive, Pasadena, CA, 91109, Mail Stop 125-109, Member AIAA.

channel and the thruster plume (including the hollow cathode) have either been impossible or have yielded unsatisfactory results. This poses a risk in the development and life qualification of long-life Hall thrusters.

The operational principle of these thrusters produces important physics not only in all three dimensions but also at time scales associated with the electron motion. Yet fully kinetic or particle-based simulations in three dimensions, aimed at tracking both electron and ion dynamics, are simply too intensive even with the current advancements in computational processing power. We are therefore constrained to two dimensions and to fluid or hybrid (fluid-particle) methods. Typically, all these methods treat electrons as a fluid in which a form of Ohm's law incorporates an anomalous contribution to the electron mobility. Though simulations in z-θ plane can provide detailed insight into instabilities with wavevector in the $\mathbf{E}\times\mathbf{B}$ direction, they provide limited information on plasma-wall interactions which are known to affect both the performance and, of course, the life of the thruster. Therefore, r-z (axisymmetric) solvers offer the only feasible approach to supporting life qualification of Hall thrusters for NASA science missions like ARRM. In response to this need the development of the 2-D axisymmetric code Hall2De began several years ago [6]. The code solves the conservation equations for the plasma in Hall thrusters on an r-z magnetic-field-aligned mesh (MFAM). But, as with all other r-z Hall thruster codes, electron transport cannot yet be determined from first principles. Instead, an anomalous collision frequency is incorporated in Ohm's law with a spatial variation that has been determined by plasma measurements. Though this approach does not provide a fully-predictive capability it can, nevertheless, provided extremely useful insight into a variety of processes in Hall thrusters and guide thruster design [7, 8]. Of importance to this article is that the spatial variation of the anomalous collision frequency in Hall2De's Ohm's law solver, which reproduces as accurately as possible the plasma measurements, has been isolated. The significance of this is that the numerical solution can be used to test the validity of theories associated with the anomalous transport in these devices before they are implemented as first-principles models in r-z electron-fluid codes.

One such theory is based on the work of Adam, et al. [9] who proposed that the turbulence generated by the electron cyclotron drift instability (ECDI) [10] is the cause of the anomalous electron transport in a Hall thruster. Their conclusions were based on the results of 2-D particle simulations in the z-θ plane and on measurements [11-13]. Coche and Garrigues reached similar conclusions from simulations with a different 2-D, z-θ particle code [14]. In this article we use Hall2De to test the fidelity of an idealized model of the ECDI-driven anomalous transport. The model is based on the hypothesis that the ECDI excites ion acoustic turbulence that enhances the effective collision frequency. It employs quasi-linear theory to relate the wave energy density to the anomalous collision frequency and assumes Maxwellian velocity distributions for electrons and ions to determine the ion acoustic wave growth and damping (Landau) rates. Only those singly-charged ions that form the ion beam are assumed to participate in the turbulence.

A brief overview of Hall2De is provided in the introduction of Section I. More detail on the plasma solutions and comparisons with measurements that are used in subsequent sections are provided in I.A. These numerical solutions are combined in Sections I.B and I.C with the aforementioned ECDI model to identify in what regions, if any, the model fails. One of the main findings of this investigation is that accounting for warm ions is of utmost importance. Therefore, two models have been incorporated in Hall2De to provide a solution for the ion temperature. Results from simulations with these models are provided in Section I.C. The article concludes with Section II.

I. Theory and Numerical Simulations in the r-z Plane

The numerical simulations presented in this paper have been performed with the Hall2De code, [6, 15] a two-dimensional (2-D), axisymmetric computational solver of the conservation equations that govern the evolution of the partially ionized gas in Hall thrusters. The governing equations, numerical methodology, various thruster simulations and comparisons with measurements have been presented elsewhere [6, 16, 17] [18] Here, we provide only a brief overview of the code for completeness.

Excessive numerical diffusion due to the large disparity of the transport coefficients parallel and perpendicular to the magnetic field is evaded in Hall2De by discretizing the equations on a computational mesh that is aligned with the applied magnetic field. Typically, the MFAM spans a computational domain in r-z geometry that extends several times the thruster channel length in the axial direction, and encompasses the cathode boundary and the thruster centerline [Fig. 1-left]. All simulations in this article have been performed for the unshielded version of the 6-kW Hall thruster called the H6 [19] [Fig. 1-right] at 300 V and 20 A of discharge voltage and current, respectively. In these simulations the near-plume computational domain spanned approximately 3 and 6 times the acceleration channel length in the radial and axial directions, respectively. The solution of the electron energy conservation equation provides T_e. Ohm's law is solved in the frame of reference of the magnetic field with the electrical resistivity accounting for contributions from collisions of electrons with all other species. The conservation equations for the electrons are closed with boundary conditions (BC) at all surfaces. The channel (ring) walls are dielectrics emulating the H6 thruster design. For all dielectric-wall boundaries a zero-current condition is imposed. At these surfaces the BC for the convective heat loss follows the formulations of Hobbs and Wesson [20] for the potential drop in a sheath with secondary electron emission. At the anode we impose (conducting) sheath BCs for the electron current density normal to the anode. At the cathode boundary the neutral particle flux, ion flux, plasma potential and electron temperature are specified. The far plume solution is subject to outflow BCs. The energy equation is solved in a semi-implicit fashion; the thermal conduction term is implicit whereas all other terms are evaluated explicitly. Current conservation, incorporating Ohm's law to solve for the electron current density, is also solved implicitly.

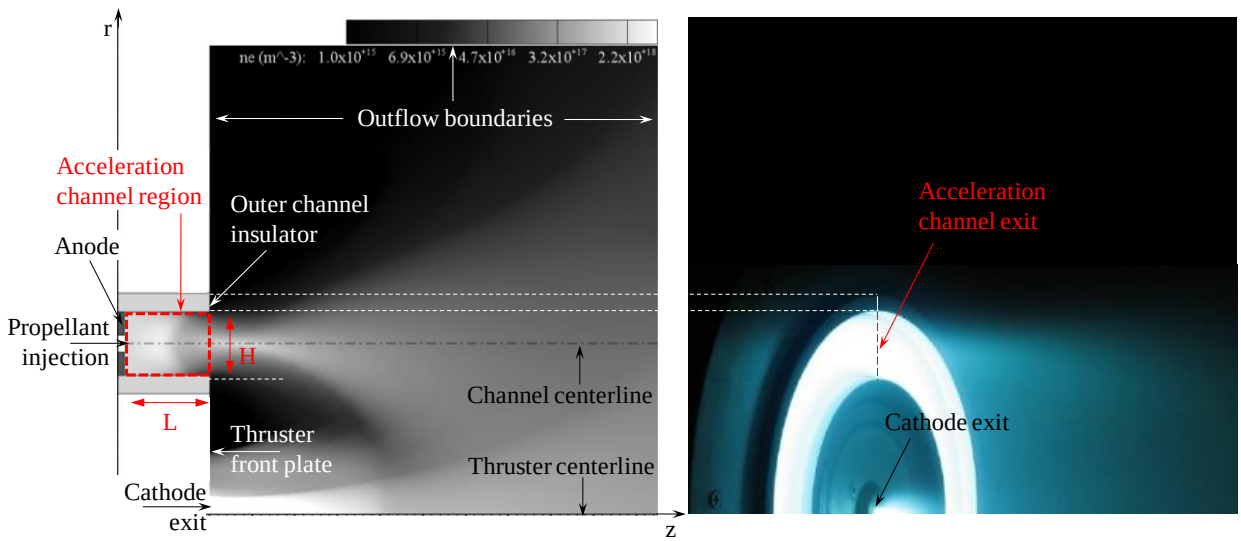

Fig. 1. Left: Computational domain of a H6 Hall thruster showing naming conventions for various thruster components and boundaries. Right: Photograph of the H6 laboratory Hall thruster operating in a vacuum facility.

The numerical solution of the conservation equations for the heavy species is obtained without invoking discrete-particle methods. The evolution of the (collision-less) neutral species is computed using line-of-sight formulations that account for ionization [15]. Ions have so far been treated in Hall2De as an isothermal, cold (relative to the electrons) fluid, accounting for the drag force and the ion-pressure gradient. As part of the work presented in this article, we have incorporated two different models to capture the evolution of the ion temperature. The models and results from our first simulations of the ion temperature are presented in Section I.C. The algorithm for the ion hydrodynamics employs a semi-implicit, conservative, cell-centered scheme that allows for better accuracy and reduced computation times. Inter-cell fluxes are determined using a variant of the Harten-Lax-van Leer (HLL) scheme [21]

and is described in more detail in [18]. The equations of motion for ions are discretized in time using a semi-implicit predictor/multi-corrector [22] scheme that has shown to reduce Hall2De computation times by 3-4 times.

One of the principal drawbacks of employing continuum formulations compared to particle methods (like particle-in-cell) for simulating the flow of ions is the inability to resolve distinct ion populations. Though the relaxation times for ions can be shown to be small enough inside the acceleration channel, such times can become exceedingly high in the near plume region. Here slow ions from the cathode combined with slow ions generated in this region by ionization and charge exchange collisions have highly disparate transit times compared to the beam ions coming from the acceleration channel. If modeled as a single fluid, convection of slow ions in the near plume will occur at the mean velocity, which is dominated by the momentum of the fast ions. This would in turn result in erroneously low particle densities in regions that reside outside that main beam expansion, such as those near the thruster poles for example [23]. The novel approach implemented in Hall2De makes uses of a multi-fluid algorithm [6, 24]. Determination of the fluid to which a given ion belongs is made upon examining the plasma potential at the location where the ion mass element was generated. The present simulations allow for two distinct ion populations: the main-beam ions and "slow" ions generated at regions where the potential is ≤50 V. Up to triply charged ions are accounted for each of the two fluids yielding a total of 6 ion momentum equations. It is emphasized that though two populations are accounted for, the ECDI model is applied only to the singly-charged main-beam population.

A. **Anomalous Collision Frequency Derived from Measurements and Simulations**

In light of the elusive nature of the physics behind the anomalous transport of electrons in Hall thrusters, a focused effort that now spans several years has been dedicated to isolating the spatial variation of the anomalous collision frequency both inside and outside the acceleration channel. The main motivation behind this is that if the spatial variation of the additional collision frequency necessary in Ohm's law can be identified, the path towards identifying the physics that produce it could be more straightforward. If this frequency allows the simulations to reproduce fully the plasma measurements then it may be as valuable as a direct measurement. We emphasize "fully" because it would not be helpful (in fact it could be misleading) if the identified collision frequency yielded back only parts of the available plasma measurements and/or performance.

We have focused mainly on one Hall thruster, namely the H6US, to take advantage of the many measurements that have been performed in this thruster over the years by different investigators at various institutions of government and academia. These measurements were then used in numerical simulations with Hall2De in which the specification of the anomalous collision frequency was not confined to one or two coefficients associated with loosely defined "thruster regions" (as done in the HPHall code for example [25]). Instead, we use several coefficients which are not linked to any specific region of the thruster. This not only allowed for the determination of a profile that yielded the most accurate reproduction of the measurements to-date, but also revealed sensitivities of the plasma to variations in the collision frequency not fully appreciated in the past. One such sensitivity that is relevant to this investigation is illustrated in Fig 2 below. The plot summarizes the results of several simulations with Hall2De performed a few years ago. Plotted are the plasma potential (left) and electron temperature (right) along the channel centerline for several values of f_0, one of the several coefficients used in the specification of the anomalous collisions frequency. This coefficient controls mainly the magnitude of the collision frequency upstream of the location where the majority of the potential drop occurs. All the different cases plotted in Fig 2 yield approximately the correct discharge current for the simulated operating condition. These simulations show that the response of the interior plasma to very large variations of the collision frequency there is relatively small. Unfortunately, in most cases, these small differences are within the uncertainly of the plasma measurements in this region. The consequence is that much of the interior ($z/L \lesssim 0.65$) variation of the collision frequency is more ambiguous than in downstream regions of the channel where the main acceleration and expansion of the ions occurs. Though plasma measurements offer little insight on the anomalous collision frequency in this interior region of

the channel, some guidance from thruster performance measurements may be used to reduce our large uncertainty. Specifically, the simulations show that a lower value of f_0 produces better agreement with the measured thrust but at the expense of a worst agreement with the few measurements of electron temperature available in this region. The reasons that a lower collision frequency in the interior produces more thrust are well understood but are beyond the scope of this paper.

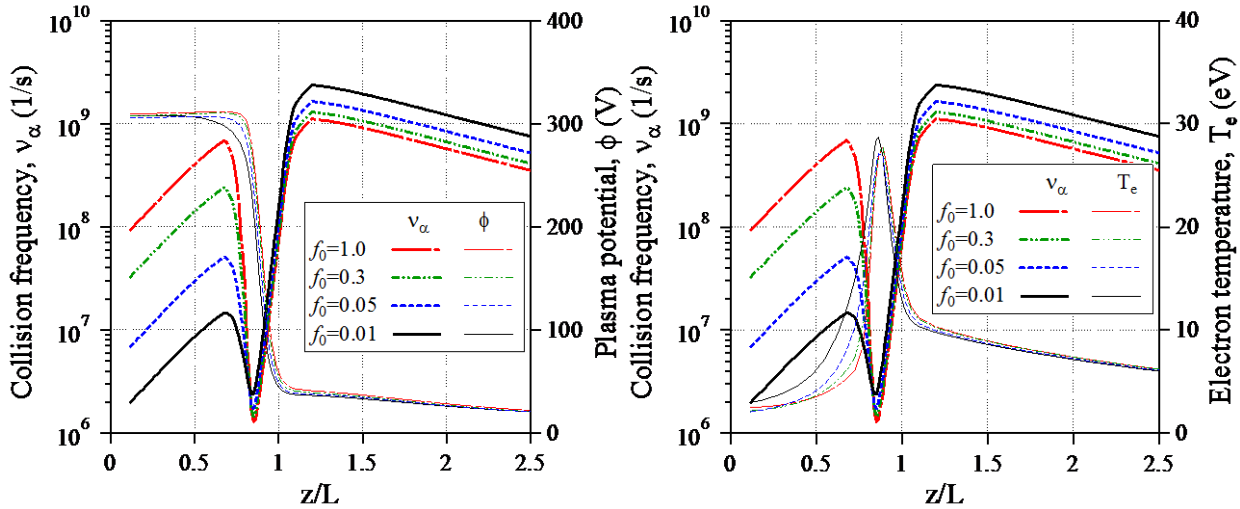

Fig 2. Sensitivity investigations with Hall2De on the effects of large variations of the anomalous collision frequency in the interior of the acceleration channel. Left: Plasma potential (ϕ) and anomalous collision frequency along the channel centerline. Right: Electron temperature (T_e) and anomalous collision frequency along the channel centerline.

Matters are further complicated by uncertainties in the measurements that are associated with the location of the acceleration region. This is best illustrated in Figs 3 and 4. Plotted are measurements of the plasma potential obtained using (a) emissive probes injected into the plasma [26] and (b) Laser Induced Fluorescence (LIF) diagnostics [27]. It should be noted that these measurements were performed in different versions of the same thruster (but at the same operating condition) and by different investigators at different facilities. Yet, the agreement between these measurements is excellent. However, measurements of the electron temperature using an injected Langmuir probe along the channel centerline and wall probes [26] (from which the measured values were extrapolated along magnetic field lines onto the centerline), introduce some ambiguity on the precise location of the acceleration region. Specifically, referring to the measurements only, maximum heating of the electrons appears to occur in a region where the electric field **E**~0. It is widely accepted that work done by the electric field on the electrons (appearing as $\mathbf{E}.\mathbf{j}_e$ in the electron energy equation) is the main source of heat for these electrons. The simulations support this conclusion. Shown in Fig 3 is a Hall2De simulation we will term hereinafter as "N" (for nominal) with a collision frequency specified in a way that closely reproduces the measured electron temperature. In this solution the acceleration region is found to be upstream of that measured by the emissive probe and LIF, in accordance to the volumetric heating imposed by $\mathbf{E}.\mathbf{j}_e$. Here it should be noted that both convection and thermal diffusion of the electron energy flux are accounted for in the simulations.

In light of this discrepancy, a second simulation has been performed, termed "F" (for Forward), which places the anomalous collision frequency downstream of that in Simulation N, in a manner that reproduces well the measured plasma potential. The results are plotted in Fig 4. In this simulation the location of the peak electron temperature is now downstream of that measured, again, as dictated by the computed volumetric heating imposed by $\mathbf{E}.\mathbf{j}_e$. It should be noted that even though measurements by injected Langmuir probes are now known to perturb the plasma [28, 29], probes imbedded in the walls of the thruster are not subject to the same impediment. The pair of simulations, therefore, quantifies our

spatial uncertainty on the location of the acceleration region and peak electron heating. This amounts to $\pm z/L \approx 0.25$.

Despite the uncertainties described in these last few paragraphs, the combination of measurements and plasma simulations presented in this section identify a solution range for the plasma in this thruster that, we believe, achieves the most accurate representation of the plasma in this thruster. The major advantage offered by these solutions is that they can be used to test different theories of the physics driving anomalous electron transport before considerable time is dedicated to their implementation in r-z codes like Hall2De. In the ensuing sections we use Simulations N and F to assess the validity of the **E**x**B**-driven ion acoustic instability proposed to drive the anomalous transport of electrons in Hall thrusters.

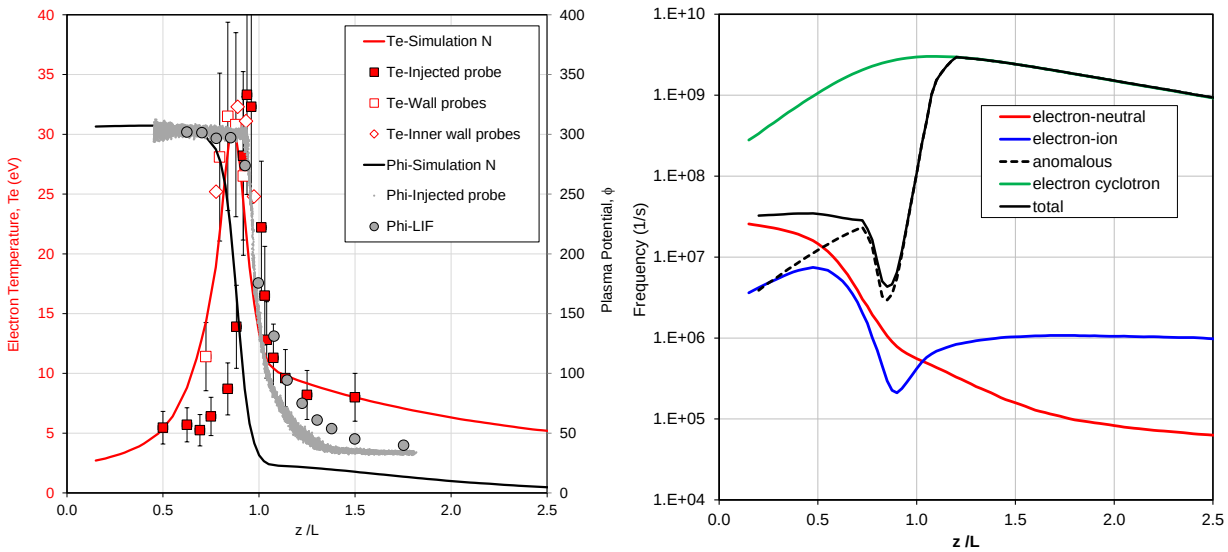

Fig 3. Hall2De "Simulation N." Left: Comparison between measurements and simulations of the electron temperature and plasma potential along the channel centerline. Right: Variation of collision frequencies compared to the electron cyclotron frequency. The anomalous collision frequency is imposed whereas the classical frequencies (electron-neutral and electron-ion) are computed.

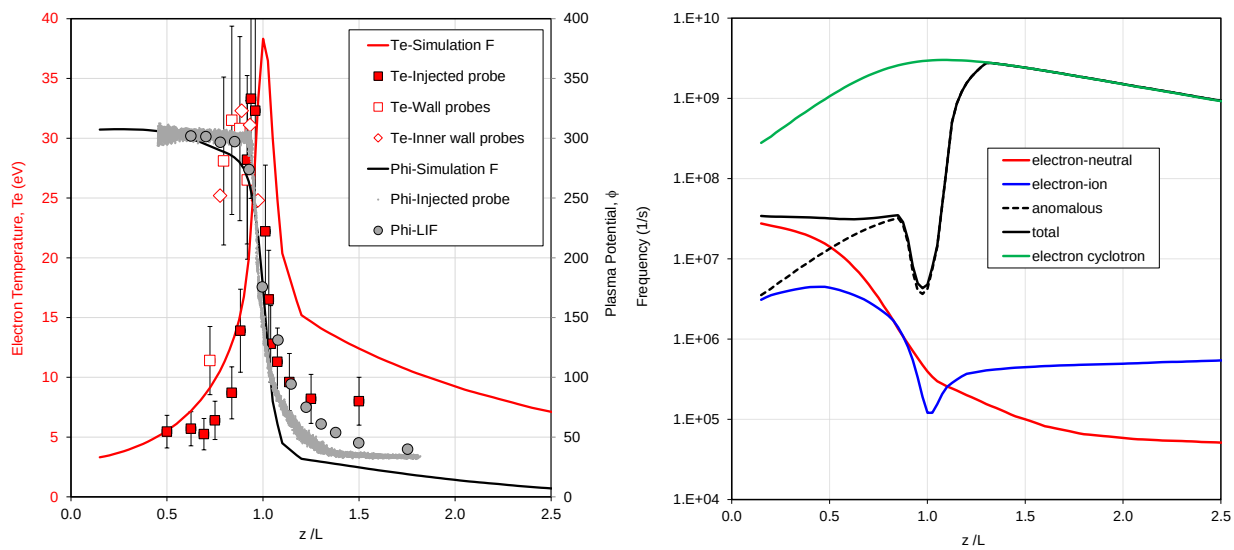

Fig 4, Hall2De "Simulation F." Left: Comparison between measurements and simulations of the electron temperature and plasma potential along the channel centerline. Right: Variation of collision frequencies compared to the electron cyclotron frequency. The anomalous collision frequency is imposed whereas the classical frequencies (electron-neutral and electron-ion) are computed.

B. **Total Growth Rate Derived from Measurements and the Wave Evolution Equation**

It is possible to gain considerable insight into the growth rate physics based on the solutions of Simulations N and F presented in the previous section. Fist we define the total wave energy density W of an isotropic turbulence spectrum,

$$W = \int W_k dk \tag{1}$$

with W_k denoting the energy density corresponding to a range dk of wavenumbers ($|\mathbf{k}|=k$). For ion-sound turbulence we use the relation

$$W = \frac{\varepsilon_0}{2}|\delta E|^2 \omega_r \left.\frac{\partial \varepsilon}{\partial \omega}\right|_{\omega=\omega_r} \tag{2}$$

where ω_r is the real part of the ion-sound wave frequency ω, $|\delta E|$ represents the electric field fluctuations and ε is the dielectric function, which in general may be written as:

$$\varepsilon(\mathbf{k},\omega) = 1 + \sum_{j=e,i} \frac{\omega_{pj}}{k^2} \int \frac{\mathbf{k}\cdot \partial f_j / \partial \mathbf{v}}{\omega - \mathbf{k}\cdot\mathbf{v}}, \qquad \omega = \omega_r + i\gamma\,. \tag{3}$$

In Eq. (3) ω_{pj} is the plasma frequency and f_j is the velocity distribution function (VDF) for species j. For a Maxwellian VDF for electrons drifting across a Maxwellian ion distribution, the effective frequency of collisions between them and the ion-sound waves can be derived from quasi-linear theory and the dispersion function for ion sound waves, to yield eventually the collision frequency [30],

$$\nu_\alpha \approx \omega_{pe} \frac{W}{e\, n_e T_e}\,. \tag{4}$$

Given then the anomalous collision frequency derived from the measurements a corresponding "measured" wave energy density can determined directly from Eq. (4). We assign subscript "m" to this quantity to signify that it is (indirectly) derived from the measurements, that is:

$$W_m \equiv \frac{\nu_\alpha}{\omega_{pe}} e\, n_e T_e\,. \tag{5}$$

W_m is the dashed line in Fig 5. The plasma properties needed in Eq. (5) to evaluate W_m were taken from the Hall2De Simulation N (Fig 3). A conservation equation for the evolution of the wave energy may be derived from the wave kinetic equation for the density distribution $N(t,\mathbf{r},\mathbf{k})=W(t,\mathbf{r},\mathbf{k})/\omega(t,\mathbf{r},\mathbf{k})$ representing the wave action associated with the propagation of wave packets (also known as quasi-particles). The derivation is beyond the scope of the paper but the interested reader is referred to Ref. [31].

$$\frac{\partial W}{\partial t} + \nabla\cdot\left(W\,\mathbf{v}_g\right) = 2\gamma W \tag{6}$$

The real part of the wave frequency for sound waves associated with ions drifting with velocity $\mathbf{u}_i$ is given by,

$$\omega_r = \mathbf{k}\cdot\mathbf{u}_i + \frac{kC_s}{\sqrt{1+k^2\lambda_D^2}} \tag{7}$$

and the group velocity $\mathbf{v}_g$ may therefore be approximated as

$$\mathbf{v}_g = \frac{\partial\omega_r}{\partial\mathbf{k}} = \mathbf{u}_i + \hat{\mathbf{k}}\frac{C_s}{\left(1+k^2\lambda_D^2\right)^{3/2}} \approx \mathbf{u}_i \tag{8}$$

when $|\mathbf{u}_i|$>>Cs (which is valid for beam ions). In Eq. (8), C_s and λ_D are the ion acoustic speed and Debye length, respectively.

Then, in steady state and assuming a single fluid consisting of singly-charged ions with drift $\mathbf{u}_i^+$, Eq. (6) can be used to define a total growth rate γ_m as follows:

$$\gamma_m \equiv \frac{\nabla\cdot\left(W_m\,\mathbf{u}_i^+\right)}{2W_m}. \tag{9}$$

We note that, as with W, we have used subscript "m" in the symbol for the growth rate. This is to signify that the quantity is derived from simulation results that yield the best agreement with measurements by adjusting the spatial variation of the anomalous collision frequency ν_α as shown in [Fig 3 & 4]. In light of the aforementioned uncertainty associated with variation of the anomalous collision frequency deep in the interior of the channel, we can attempt to solve Eq. (6) using γ_m and an initial condition for the wave energy density representing the starting noise level for the instability. This then would arguably provide a more physical representation of the variation of W in this region of the thruster. We specify the initial energy density W_0 as

$$W_0 = \delta e n_{e0} T_{e0} \tag{10}$$

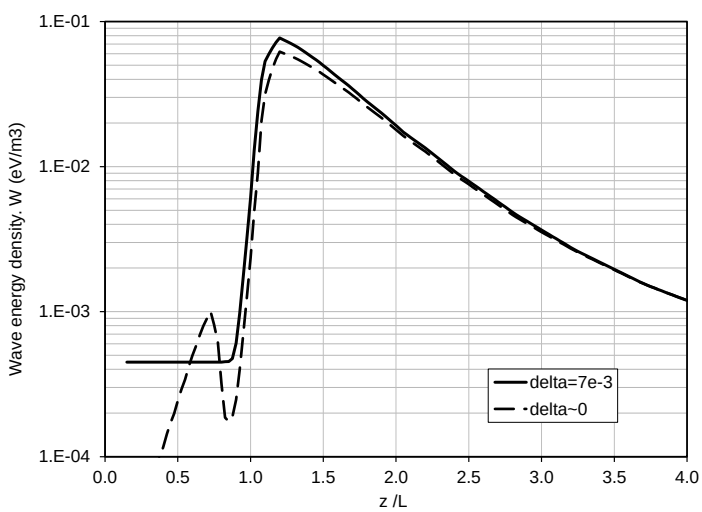

Fig 5. Dashed solution: Wave energy density that would be required to produce the measured plasma behavior in Fig 3 (from Eq. (5)). Solid solution: Steady state Hall2De solution of the time-dependent plasma equations and the wave equation, $\partial W/\partial t + \nabla\cdot\left(W\mathbf{u}_i^+\right) = 2\gamma_m W$, with a floor noise level W_0.

where δ determines the noise level and $en_{e0}T_{e0}$ is a reference energy density value (Fig 5) with n_{e0}=2e17 m^{-3} and T_{e0}=2 eV. These are representative values of plasma conditions in the near anode region. Then we evolve numerically Eq. (6) as part of the overall system of conservation laws in Hall2De. The steady state solution is shown in Fig 6 after the nominal discharge current of 20 A has been approximately achieved. For this solution we have used δ=7e-3. As expected the only differences in the wave energy density between solution of Eq. (6) and the value given directly by Eq. (5) is exhibited in the anode region, as shown in Fig 6. The effect of W_0 on the anomalous collision frequency ν_α and the rest of the plasma solution is, as expected, also exhibited only in this region of the thruster. The overall effect is to smooth out the non-monotonic step-like features of ν_α (e.g. see Fig 3) but at the same time widen the electron temperature profile and increase the interior electric field. These effects have also been expected based on the discussion in the previous section (Fig 2).

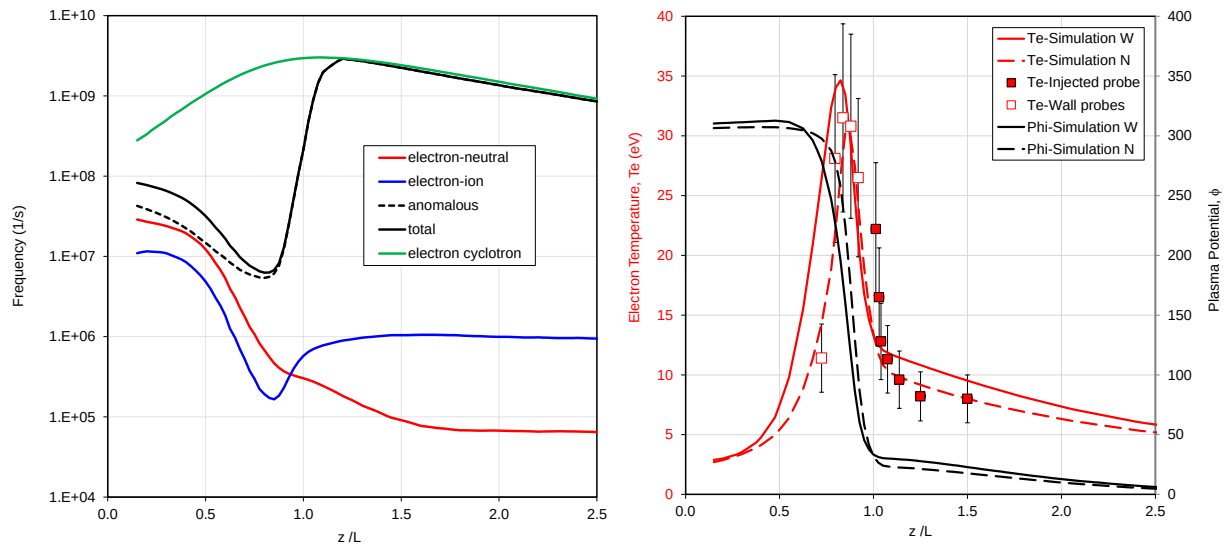

Fig 6. Hall2De Simulation W. Steady state Hall2De solution of the time-dependent plasma equations and the wave equation, $\partial W/\partial t+\nabla\cdot\left(W\mathbf{u}_i^+\right)=2\gamma_m W$, subject to an initial wave energy density level given by Eq. (10), where δ=7e-4, n_{e0}=2e17 m^{-3} and T_{e0}=2 eV.

C. Validity of the Fluid Model of E×B-Driven Ion Acoustic Instability in the r-z Plane

The total growth rate in Eq. (6) consists of destabilizing and stabilizing terms

$$\gamma=\gamma_D-\left(\gamma_L+\nu_i\right), \tag{11}$$

where the destabilizing contribution (γ_D) assumes Maxwellian electrons with drift velocity u_{de} in the **E**×**B** direction (also chosen to be the direction of the wavevector $\mathbf{k}=ke_{ExB}$). Landau damping (γ_L) assumes Maxwellian ions. Under these assumptions and for $u_{de}<<u_{Te}=(2eT_e/m_e)^{1/2}$ the two terms are mathematically identical to the classical expressions of the ion acoustic instability [32], excited (or damped) by drifting electrons in a background of Maxwellian ions. They are as follows, for γ_D

$$\gamma_D=\sqrt{\frac{\pi}{8}}\frac{|\omega_r|}{\left(1+k^2\lambda_D^2\right)^{3/2}}\left(\frac{u_{de}}{C_s}\sqrt{1+k^2\lambda_D^2}-1\right)\sqrt{\frac{m_e}{m_i}} \tag{12}$$

and for γ_L,

$$\gamma_L = \sqrt{\frac{\pi}{8}} \frac{|\omega_r|}{\left(1+k^2\lambda_D^2\right)^{3/2}} \left(\frac{T_e}{T_i}\right)^{3/2} \exp\left[-\frac{T_e}{2T_i\left(1+k^2\lambda_D^2\right)}\right]. \tag{13}$$

With the wavevector in the **E**x**B** direction the real part of the wave frequency takes the form

$$\omega_r = \frac{\omega_{pi}}{\sqrt{1+1/k^2\lambda_D^2}} = \frac{kC_s}{\sqrt{1+k^2\lambda_D^2}} \tag{14}$$

where ω_{pi} is the ion plasma frequency. In all subsequent Hall2De simulations collisional damping of ions is accounted for by the frequency ν_i which accounts for all collisions between the singly-charged ion population (participating in the wave motion) and ions of higher charge, self-collisions, as well as collisions with neutrals:

$$\nu_i = \sum_s \nu_{is}, \qquad s = Xe, Xe^+, Xe^{++}, Xe^{+++}. \tag{15}$$

Though the simulations have been conducted by assuming two distinct ion fluids (see description of multi-fluid approach in Hall2De in [6, 24]), no damping due to collisions between the two fluids has been included. The second fluid consists of "slow" ions generated in regions where the plasma potential is ≤50 V. In principle, the wavevector magnitude k can (and probably does) vary which would require an additional conservation equation to capture its evolution. As a first approximation we assume that $k\lambda_D=1/\sqrt{2}$, which maximizes the destabilizing growth in the absence of damping. Using a combination of numerical simulations and measurements we can then assess the validity of the theoretical destabilizing growth rate given in Eq. (12). Specifically, using the computed values of the **E**×**B** drift, ω_{pi} and C_s we compare the result from Eq. (12) with the sum

$$\gamma_m + \gamma_L + \nu_i \tag{16}$$

where, in this first set of comparisons we assume that the ions are cold. That is, γ_L in the above sum is determined by Eq. (13) using the Hall2De-computed ω_{pi} and T_e while the ion temperature is taken to equal that of neutrals, T_i=0.07 eV. A close agreement between the values in Eq. (12) and sum (16) would strengthen the argument for the **E**×**B**-driven ion acoustic instability and suggest that a fully self-consistent numerical solution in the r-z plane using the Eqs. (6) and (12)-(15) may be possible.

The comparison between the two results is shown in Fig 7-left for Simulation N. Also plotted for reference are the total growth rate γ_m and the ion collision frequency ν_i. These show that Landau damping is of little significance here since the necessary destabilizing growth needed must largely counter collisional damping and, to some extent in the vicinity of the channel exit, the convection of the wave energy. The comparison between the theoretical value of γ_D in Eq. (12) and the sum in (16) shows little to no correlation. The theoretical value over-predicts the growth of these waves in the range 0.7<z/L<1 and under-predicts it in the near-anode and plume regions. A somewhat better agreement is achieved in the near-anode region with the solution from Simulation F as shown in Fig 7-right. But the comparison for the remaining regions remains qualitatively the same. The result suggests that if Eqs (6) and (12)-(15) were solved self-consistently with the plasma conservation equations in Hall2De, neither of the two solutions presented in Fig 3 and 4 would have been re-produced. As stated in Section I.A., based on the measurements these solutions represent most closely the observed behavior of the plasma in the thruster.

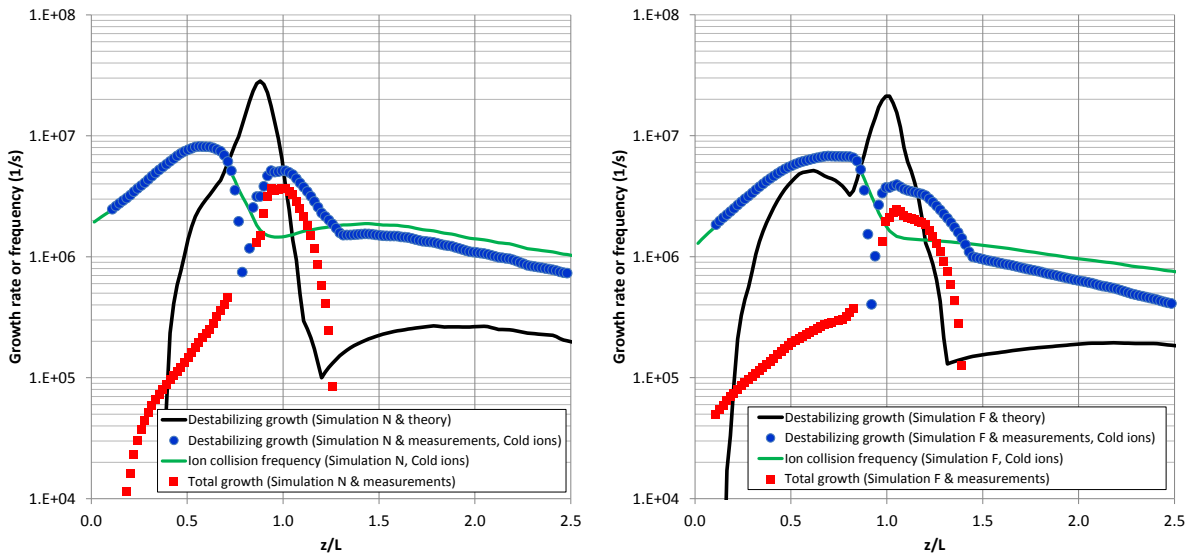

Fig 7. Comparison of the theoretical value of the destabilizing growth rate for ion acoustic waves, γ_D (Eq. (12)), with the value expected based largely on plasma measurements, $\gamma_D+\gamma_L+\nu_i$. Ions are assumed to be cold (T_i=0.07 eV). Whenever direct measurements were not available, values from the Hall2De simulations that closely reproduce the measurements were used. Left: Simulation N. Right: Simulation F.

D. Significance of the Ion Temperature

The comparisons in Fig 7 underscore the likelihood that dominant physics are missing from the theoretical model of the **E**×**B**-driven ion acoustic instability described in the previous section. Considering the sensitivity of the Landau term (γ_L) on the ion temperature we re-visit here the assumption of cold ions.

Huang et al. [27] used Laser Induced Fluorescence (LIF) diagnostics to measure the VDF of singly charged ions along the channel centerline. Though in general the VDFs did not follow a Maxwellian distribution, some appeared close enough to allow for an approximation of the ion temperature. A few representative examples with fits using a drifting Maxwellian are provided in Fig 8. The drift velocity was taken directly from the VDF measurement at approximately the location were the measured intensity was unity. Examples of measured VDFs with deviations from a Maxwellian VDF that were deemed too large to allow for an extraction of the ion temperature are provided in Fig 9.

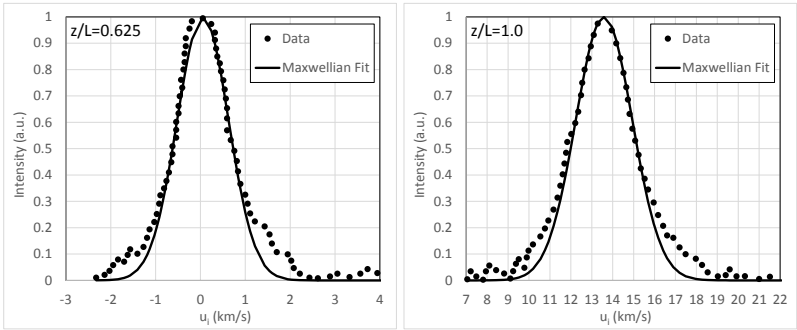

Fig 8. LIF measurements [27] along the channel centerline of the thruster for which Maxwellian fits were used to extract the ion temperature.

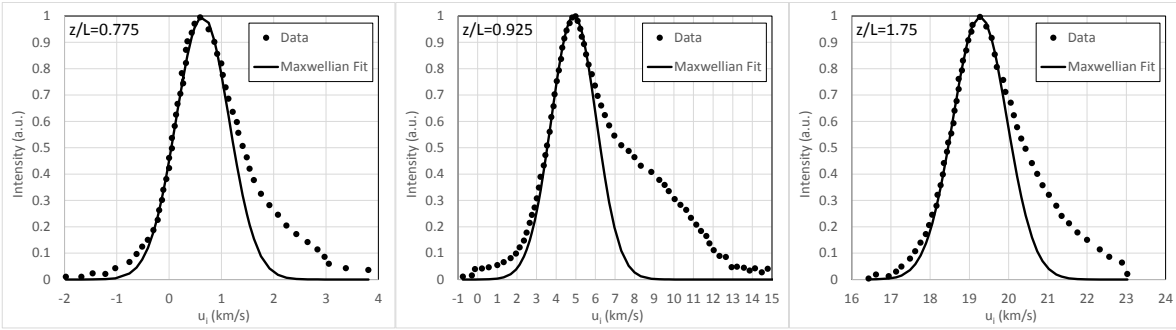

Fig 9. LIF measurements [27] along the channel centerline of the thruster for which Maxwellian fits were *not* used to extract the ion temperature.

The ion temperatures derived from the LIF measurements are plotted in Fig 10-left as a function of z/L. Also plotted for comparison are the solutions of the electron temperature from Simulations N and F. For better clarity in the comparison we also include only the near-plume data for the electron temperature from the injected probe, for which perturbation of the plasma by the probe is reduced [28]. To quantify the impact of these ion temperatures on the total growth rate, we define the non-dimensional Landau stabilizing term, at $k\lambda_D=1/\sqrt{2}$, as follows

$$\bar{\gamma}_L = \left(\frac{T_e}{T_i}\right)^{3/2} \exp\left(-\frac{T_e}{3T_i}\right), \tag{17}$$

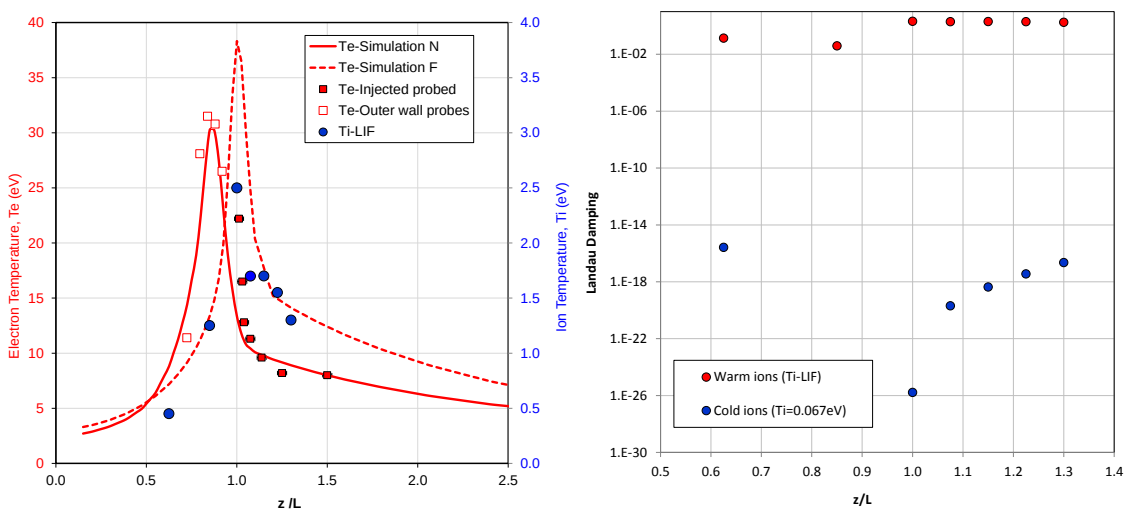

Fig 10. Left: Comparison between electron and ion temperatures along the channel centerline. Right: Comparison of (non-dimensional) Landau damping (Eq. (17)) for warm ions (as measured by LIF) and cold ions (T_i=0.07 eV).

and present a comparison in Fig 10-right of this value for two cases: (1) cold ions for which the ion temperature is taken to be that of neutrals (Ti=0.07 eV) and (2) warm ions for which the ion temperature is taken directly from the LIF measurements. In both cases the electron temperature was taken from the results of Simulation N. Due to the exponential in Eq. (17), the comparison yields differences of many orders of magnitude between cold and warm ions which underscore the significance of accounting for the ion temperature in r-z simulations. It should be recognized here that this sensitivity is largely due to the assumption of Maxwellian ions; non-linear damping processes and non-Maxwellian ions would alter the

form of Eq. (13) and therefore the result in Fig 10-right. However, here, the objective is to assess the promise of the idealized model of the instability which is based on quasi-linear growth of the ion acoustic waves in a Maxwellian plasma.

Accounting for the ion temperature changes significantly the comparison between the destabilizing growth rates. As in Fig 7, Fig 11 below compares the theoretical result from Eq. (12) but now with the reference or "measured" destabilizing growth, $\gamma_m+\gamma_L+\nu_i$, where the last two terms are determined using the LIF-measured ion temperatures. We now observe that the theoretical value γ_D (Eq (12)) falls between the "measured" growth rate in the channel interior. This implies that, in principle, the physical model of singly charged ions participating in ion wave growth due to the **E**×**B** drift of the electrons is plausible. But we also observe that γ_D (Eq (12)) would have to be significantly higher in the near plume due largely to Landau damping of the waves there. Collisional damping here assumes a negligible role. The variation of γ_m also is much lower than γ_L in this region. This implies that the hypothesis posed in previous work by the authors about the significance of the convection of wave energy (second term in Eq (6)) in the determination of the increasing anomalous collision frequency in this region, can no longer be supported. The much larger growth compared to Eq. (12) that is required in the region close to the thruster exit plane implies that either (a) this instability is not inhibited by classical Landau damping or, (b) that a different instability altogether, also insusceptible to Landau damping, is active here. A conjecture in support of (a) that involves slow (cold) ions generated by ionization and charge exchange is made by Katz et al. [33] in a companion paper. The conjecture is based on the assumption that this slow-ion population is not subject to Landau damping.

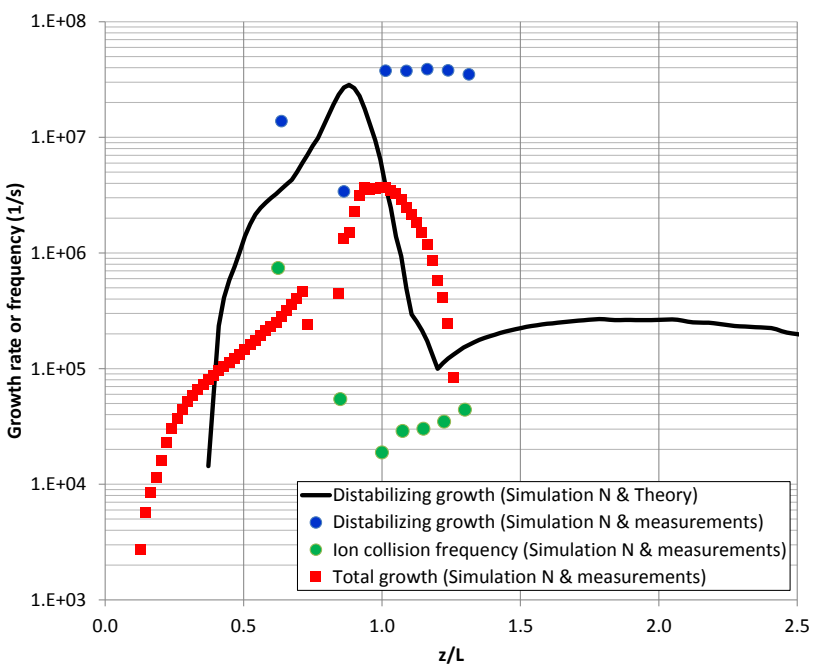

Fig 11. Comparison of the theoretical value of the destabilizing growth rate for ion acoustic waves, γ_D (Eq. (12)), with the value expected based largely on plasma measurements, $\gamma_D+\gamma_L+\nu_i$. The ion temperature was taken directly from the LIF measurements. Whenever direct measurements were not available, values from the Hall2De Simulation N were used.

Motivated by the abovementioned findings, we have incorporated in Hall2De a solver for the solution of the (classical) ion energy equation. We present here the derivation of the final form of the conservation equation incorporated in the code and some first simulation results. Conservation of the total energy for species α in a partially ionized gas is given by [34]

$$\frac{\partial}{\partial t}\left(n_\alpha\varepsilon_\alpha+\frac{3}{2}p_\alpha\right)+\nabla\cdot\left(n_\alpha\varepsilon_\alpha+\frac{5}{2}p_\alpha\right)\mathbf{u}_\alpha+\nabla\cdot\boldsymbol{\theta}_\alpha=q_\alpha n_\alpha\left(\mathbf{E}+\frac{m_\alpha\mathbf{R}_\alpha}{q_\alpha n_\alpha}\right)\cdot\mathbf{u}_\alpha+Q_\alpha \tag{18}$$

where $\varepsilon_\alpha=½m_\alpha u_\alpha^2$ is the kinetic energy, $p_\alpha=n_\alpha k_B T_\alpha$ is the pressure, n_α is the number density, $\mathbf{u}_\alpha$ is the velocity, $\boldsymbol{\theta}_\alpha$ is the conduction heat flux, q_α is the charge, $\mathbf{E}$ is the electric field. In Eq. (18) we have neglected radiative losses. Quantities Q_α and $m_\alpha\mathbf{R}_\alpha$ denote the heat generated and mean change of momentum respectively, in species α as a consequence of collisions with other species (β). These quantities in general include contributions from both elastic and inelastic collisions:

$$\begin{aligned} Q_\alpha &= \sum_\beta Q_{\alpha\beta} & Q_{\alpha\beta} &= \int\frac{m_\alpha v_\alpha^2}{2}\dot{f}_{\alpha\beta}d\mathbf{v}_\alpha\Big|_{elastic}+\int\frac{m_\alpha v_\alpha^2}{2}\dot{f}_{\alpha\beta}d\mathbf{v}_\alpha\Big|_{inelastic} \\ m_\alpha\mathbf{R}_\alpha &= \sum_\beta m_\alpha\mathbf{R}_{\alpha\beta} & m_\alpha\mathbf{R}_{\alpha\beta} &= \int m_\alpha\mathbf{v}_\alpha\dot{f}_{\alpha\beta}d\mathbf{v}_\alpha\Big|_{elastic}+\int m_\alpha\mathbf{v}_\alpha\dot{f}_{\alpha\beta}d\mathbf{v}_\alpha\Big|_{inelastic} \end{aligned} \tag{19}$$

In Eq. (19), $\dot{f}_{\alpha\beta}$ denotes the rate of change of the distribution function due to collisions between species α and β. Conservation of particles and momentum in the absence of viscous effects are by given by Eqs (20) and (21), respectively:

$$\frac{\partial n_\alpha}{\partial t}+\nabla\cdot\left(n_\alpha\mathbf{u}_\alpha\right)=\dot{n}_\alpha \tag{20}$$

$$\frac{\partial}{\partial t}\left(nm\mathbf{u}\right)_\alpha+\nabla\cdot\left(nm\mathbf{uu}\right)_\alpha=q_\alpha n_\alpha\mathbf{E}-\nabla p_\alpha+m_\alpha\mathbf{R}_\alpha\,. \tag{21}$$

where $\dot{n}_\alpha$ is the ionization rate. Expanding the left-hand side of the momentum equation and taking the dot product with $\mathbf{u}_\alpha$ yields an equation for the conservation of mechanical energy,

$$n_\alpha\frac{D\varepsilon_\alpha}{Dt}+\varepsilon_\alpha\dot{n}_\alpha=q_\alpha n_\alpha\mathbf{E}\cdot\mathbf{u}_\alpha-\nabla p_\alpha\cdot\mathbf{u}_\alpha+m_\alpha\mathbf{R}_\alpha\cdot\mathbf{u}_\alpha-\varepsilon_\alpha\dot{n}_\alpha\,. \tag{22}$$

Combining Eqs (18) and (22) eliminates the kinetic energy and yields the equation for the transport of pressure (or internal energy):

$$\frac{3}{2}\frac{\partial p_\alpha}{\partial t}+\nabla\cdot\left(\frac{5}{2}p_\alpha\mathbf{u}_\alpha+\mathbf{q}_\alpha\right)-\mathbf{u}_\alpha\cdot\nabla p_\alpha=Q_\alpha+\varepsilon_\alpha\dot{n}_\alpha\,. \tag{23}$$

For singly charged ions, Eq. (23) above may be solved for the ion temperature (instead of pressure) as follows:

$$\frac{3}{2}n_i\frac{\partial T_i}{\partial t}+n_i\nabla\cdot\left(\mathbf{u}_i T_i\right)+\frac{n_i\mathbf{u}_i}{2}\cdot\nabla T_i=Q_i+\varepsilon_i\dot{n}_i-\frac{3}{2}T_i\dot{n}_i\,. \tag{24}$$

where we have neglected thermal conduction and T_i is in eV. Classical heating of ions occurs mainly due to ionization (inelastic collisions) Q_i^I and collisions with neutrals that lead to resonant charge exchange

(elastic collisions) Q_i^E. Q_i also includes heating/cooling contributions that are due to thermal non-equilibrium with electrons (at T_e) and neutrals (at T_n) but these are much smaller compared to collisional heating. Though these terms are accounted for in the simulations they are neglected here in the formulations for simplicity. Ionization and charge-exchange heating are approximated as follows:

$$
\begin{aligned}
&Q_i \approx Q_i^E + Q_i^I \\
&Q_i^E = \frac{1}{2} m_i \dot{n}_n \left(\mathbf{u}_i - \mathbf{u}_n\right)^2 \\
&Q_i^I + \varepsilon_i \dot{n}_i \approx \frac{1}{2} m_i \dot{n}_i \left(\mathbf{u}_i - \mathbf{u}_n\right)^2
\end{aligned}
\tag{25}
$$

where $\dot{n}_n$ is the charge-exchange production rate and $\dot{n}_i$ is the classical electron-impact ionization rate for singly charged ions. The boundary conditions allow for loss of the ion energy flux $\mathbf{j}_i T_i$ across the wall sheaths and the plume boundaries with $\mathbf{j}_i$ denoting the ion current density. The mathematical model described by Eqs (24) and (25) will be referred to hereinafter as the "Classical" model. It is solved explicitly in Hall2De.

Numerical simulations with the classical model yield significantly higher ion temperatures compared to the LIF measurements, as shown in Fig 12-left. A closer look at the mean free path for classical collisions between singly-charged ions, $\lambda_{ii}=u_{Ti}/\nu_{ii}$, shows that the Knudsen number, $Kn=\lambda_{ii}/L$, begins to exceed values for which the continuum approximation is valid (Kn~0.1) in the last ~30% of the channel. This is plotted in Fig 12-right. In the estimation of λ_{ii}, u_{Ti} is the ion thermal speed, $\sqrt{(2T_i/m_i)}$, with T_i in eV, and ν_{ii} is the coulomb ion-ion collision frequency. This is in contrast to the case with cold ions for which Kn is always in the continuum regime.

A highly idealized approximation is sometimes made (e.g. [33]) to account for such deviations from the classical model by reducing the collisional heating (terms in Eq. (24) above) by the probability that when new ions are generated by ionization or charge-exchange some of them escape the original ion ensemble. This reduces the contributions to the ensemble's heating. A simple model of this is to multiply the right hand side of Eq. (24) by the probability P

$$
P = 1 - \exp\left(-\nu_{ii}\ell / u_{is}\right) \tag{26}
$$

where ℓ is a characteristic length associated with the distance it takes newly-generated ions to escape the main ions and u_{is} is their speed, which is taken here to be that of neutrals. We performed two new simulations, one with ℓ=L and one with ℓ=NL, where we iterated on N until the ion temperature was comparable to the measured values in the near plume of the thruster. In the second case we found N=8.4 implying that ℓ>>L. We term these solutions as "Collisionless model" and "Collisionless model w/ iteration." We find that although the approximation in Eq (26) reduces the heating rate and, in turn, the ion temperature, the spatial variation of the solution is significantly different than that of the measurement. Specifically, the solutions yield a double-humped variation of the ion temperature along the channel centerline despite the fact that the heating exchange terms in Eq. (25) are monotonically decreasing with z/L. The reason for this may is best illustrated by the contours of ion temperature and neutral gas density in Fig 13. As ions get heated, the ion temperature exhibits a relatively large radial variation in the channel as shown in Fig 13-left. Referring to the right hand side of Eq. (24) and dividing by the ion number density, it is clear that this occurs because the main heating source for ions is proportional to $Q \sim n_e n_n \langle\sigma v_e\rangle u_i^2/n_i \approx n_n \langle\sigma v_e\rangle u_i^2$, where $\langle\sigma v_e\rangle$ is the Maxwellian-averaged cross-section. Thus more ion heating occurs near the walls than at the centerline due to the higher neutral gas density there, as shown in Fig 13-right. The higher heating at these near-wall regions is then convected downstream by the ion velocity and converges to the centerline creating the second hump in the ion

temperature as shown in Fig 12-left. The magnitude of the secondary hump is likely exaggerated due to the fluid approximation which, analogously to a pressure compression, it predicts a thermal compression in this region. This is erroneous based on the large ion mean free paths observed here (Fig 12-right).

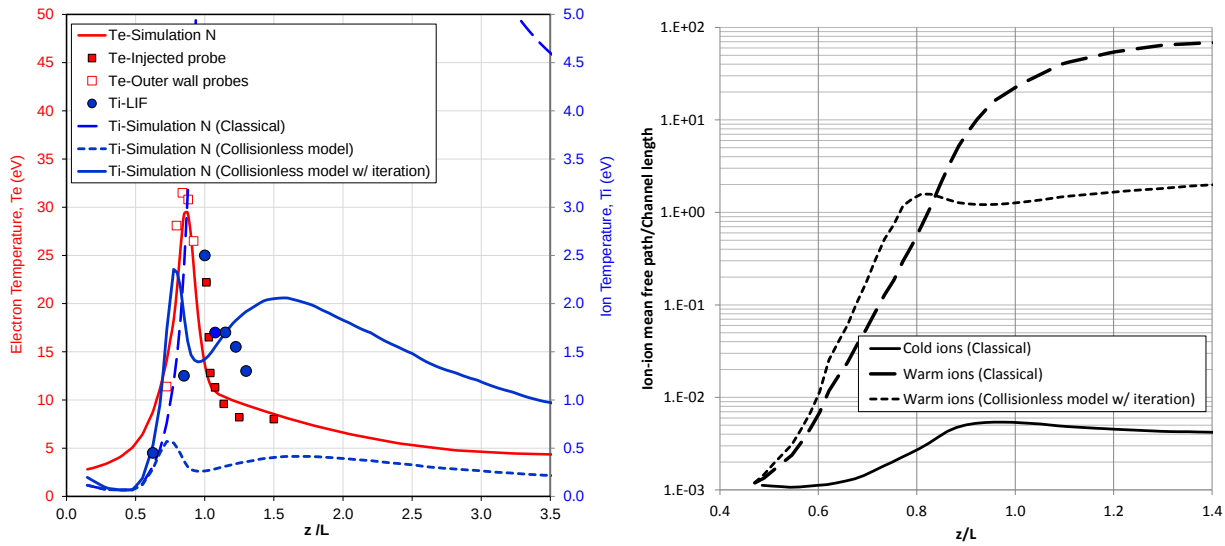

Fig 12. Left: Solutions to Eq. (24) for the ion temperature from Hall2De Simulation N and comparisons with LIF measurements along the channel centerline. Right: Computed ion-ion mean free path/channel length based on the different solutions of the ion temperature.

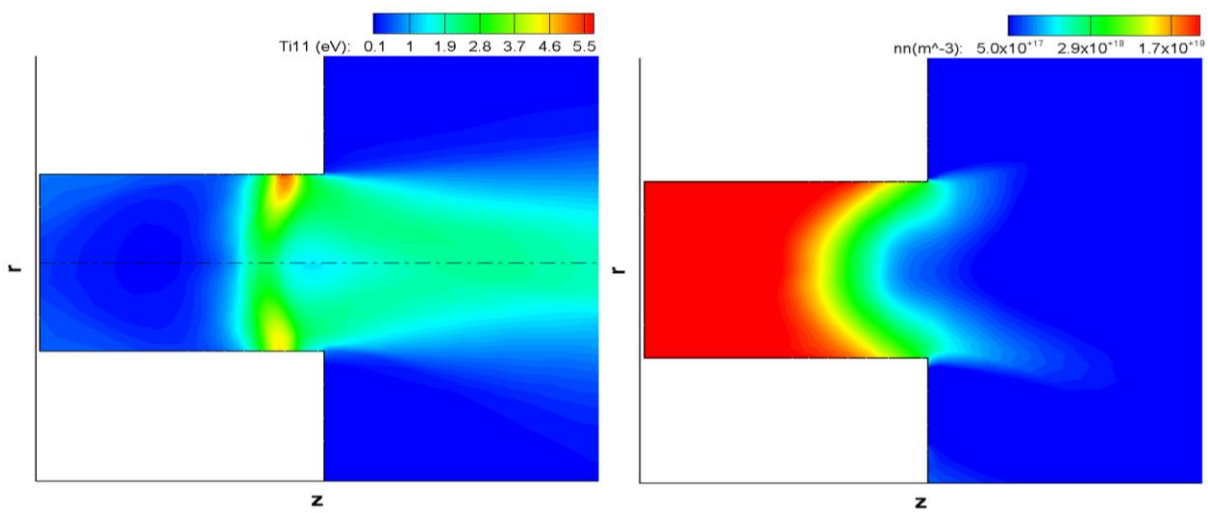

Fig 13. Left: Contours of computed ion temperature in Hall2De Simulation N using the "collision-less model w/ iteration" for the heating terms in Eq. (24). Right: Contours of computed neutral gas density.

The large deviations from collision-dominated ion flow (Fig 12-right), as exhibited by the abovementioned results on the classical ion heating and the non-Maxwellian VDFs (Fig 9), leads us to consider other means by which ions may be "heated". There is strong evidence for example to suggest that ions are heated anomalously by the instability, leading to the formation of ion tails similar to those observed in the LIF measurements [35-37]. In fact, recent measurements of the wave energy density in ion sound turbulence measured in hollow cathode discharges show a direct correlation between the ion temperature and wave energy, $\Delta T_i \sim \Delta(W/n_e)$ [38]. Moreover, theory and numerical simulations with the 2-D Orificed Cathode plasma code [39, 40] show better agreement with plasma measurements when the

model for the anomalous resistivity of the ion acoustic instability is combined with an ion energy equation that assumes the ion temperature increases proportionally to the wave energy [41, 42]. We have therefore performed another series of Hall2De simulations in which the ion temperature is determined according to

$$T_i = T_{i0} + \beta\left(\frac{W}{en_e} - \delta T_{e0}\right) \tag{27}$$

where T_{i0} and T_{e0} are reference ion and electron temperatures respectively, associated with the noise level of the instability, and β is a factor that determines the slope between T_i and W/n_e. To be consistent with the incorporation of W_0 in Eq. (27), we have used here "Simulation W" (Fig 6). The steady state results for β=2 and 3 are depicted in Fig 14. Qualitatively they exhibit better agreement with the measurement, namely a fast rise followed by a more gradual fall of the ion temperature. In light of the variation of W shown in Fig 5, this is not unexpected. Quantitatively however the fast rise occurs ~z/L=0.25 downstream of that suggested by the LIF measurements. If wave growth occurred upstream of the computed location in Simulation W and/or if the experimental error associated with the location of measurements was comparable to differences between simulation and measurement, it would explain the discrepancy in Fig 14. We note that our uncertainty in the location of the plasma as identified in Section I.A is z/L=±0.25.

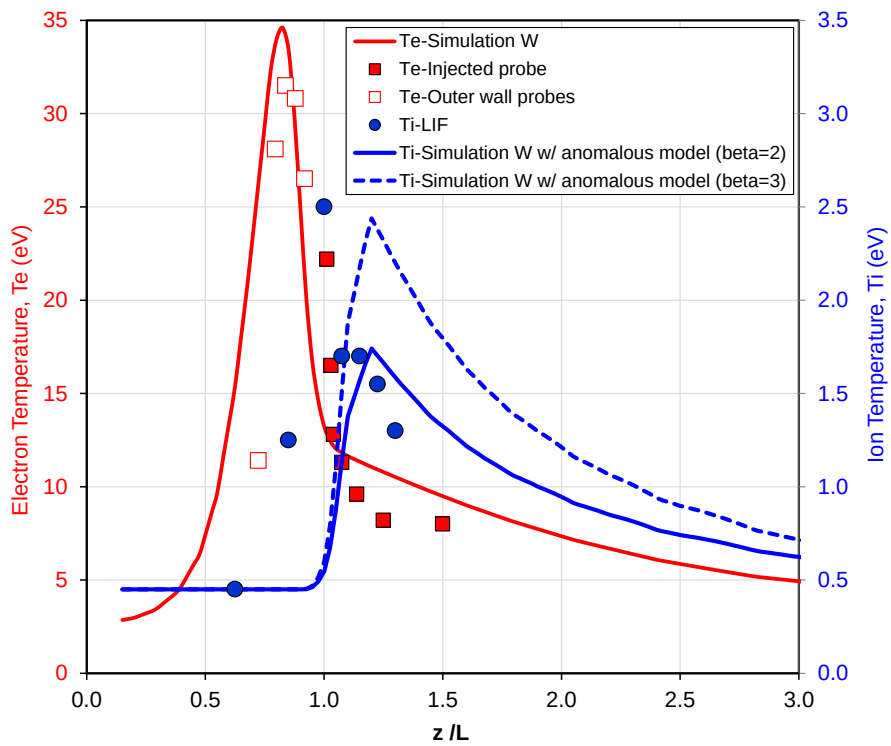

Fig 14. Solutions to Eq. (27) for the ion temperature from Hall2De Simulation W and comparisons with LIF measurements along the channel centerline.

II. Conclusions

Numerical simulations with the r-z code Hall2De have been performed to test the fidelity of an idealized model of the ECDI-driven anomalous collision frequency in a Hall thruster. The simulations have taken advantage of plasma solutions already in place after years of investigations aimed at isolating

the spatial variation of the anomalous collision frequency needed in Ohm's law to reproduce the observed plasma behavior. Though not obtained based on a self-consistent model of the anomalous frequency, these numerical solutions are as close to a measurement as one can possibly achieve in an r-z code and consequently provide a testbed for first-principles models of the anomalous transport.

By comparing the destabilizing growth rate, predicted by theory to be proportional to u_{de}/C_s (where $u_{de} \sim E_{\perp}/B$), with values derived from the measurements and these numerical solutions, we found that the idealized ECDI model fails to explain the observed behavior of the plasma when singly-charged ions comprising the main beam are assumed to be cold. When these ions are considered to be warm (based on LIF measurements) the idealized ECDI model appears more promising in the interior of the channel but fails by orders of magnitude in the near plume region due to increased Landau damping there. Convection of the wave energy generated in the channel interior is found to be insufficient to explain this discrepancy. These results imply that another mechanism is likely at play in the near plume region. In light of the significance of the ion temperature, Hall2De has been augmented with an ion energy conservation equation. However, as ions are much hotter than originally assumed the larger mean free paths between ions challenge the continuum approximation behind the derivation of the collisional heating terms. Moreover, the presence of ion tails known to exist in these thrusters poses questions about the dominant source of "heating" for these ions. Simulations assuming a linear dependence of the ion temperature on the wave energy yield somewhat more promising results based on the LIF measuremnts. Such dependence was recently measured in electric propulsion hollow cathode discharges in which anomalous resistivity due to ion acoustic turbulence in known to exist.

Acknowledgments

The research described in this paper was carried out by the Jet Propulsion Laboratory, California Institute of Technology, under a contract with the National Aeronautics and Space Administration.

References

[1] D. A. Herman, J. E. Polk, R. R. Hofer *et al.*, "The Development of the Ion Propulsion System for the Solar Electric Propulsion Technology Demonstration Mission " in 34th International Electric Propulsion Conference, Hyogo-Kobe, Japan, IEPC-2015-008, July 2015.

[2] J. R. Brophy, and B. Muirhead, "Near-Earth Asteroid Retrieval Mission (ARM) Study," in 33rd International Electric Propulsion Conference, Washington, DC, 2013.

[3] B. K. Muirhead, and J. R. Brophy, "Asteroid Redirect Robotic Mission Feasibility Study," in 2014 IEEE Aerospace Conference, Big Sky, MT, 2014.

[4] M. Gates, B. K. Muirhead, B. J. Naasz *et al.*, "NASA's Asteroid Redirect Mission Concept Development Summary," in 2015 IEEE Aerospace Conference, Big Sky, MT, 2015.

[5] D. D. Mazanek, R. G. Merrill, S. P. Belbin *et al.*, "Asteroid Redirect Robotic Mission: Robotic Boulder Capture Option Overview," in AIAA SPACE 2014 Conference and Exposition, San Diego, CA, 2014.

[6] I. G. Mikellides, and I. Katz, "Numerical simulations of Hall-effect plasma accelerators on a magnetic-field-aligned mesh," *Physical Review E*, vol. 86, no. 4, pp. 046703, Oct 17, 2012.

[7] I. G. Mikellides, I. Katz, R. R. Hofer *et al.*, "Magnetic shielding of the channel walls in a Hall plasma accelerator," *Physics of Plasmas*, vol. 18, no. 3, pp. 033501, Mar, 2011.

[8] I. G. Mikellides, I. Katz, R. R. Hofer *et al.*, "Magnetic shielding of a laboratory Hall thruster. I. Theory and validation," *Journal of Applied Physics*, vol. 115, no. 4, Jan 28, 2014.

[9] J. C. Adam, A. Heron, and G. Laval, "Study of stationary plasma thrusters using two-dimensional fully kinetic simulations," *Physics of Plasmas*, vol. 11, no. 1, pp. 295-305, Jan, 2004.

[10] D. W. Forslund, R. L. Morse, and C. W. Nielson, "Electron Cyclotron Drift Instability," *Physical Review Letters*, vol. 25, no. 18, pp. 1266-&, 1970.

[11] A. Ducrocq, J. C. Adam, A. Heron *et al.*, "High-frequency electron drift instability in the cross-field configuration of Hall thrusters," *Physics of Plasmas*, vol. 13, no. 10, Oct, 2006.

[12] S. Tsikata, N. Lemoine, V. Pisarev *et al.*, “Dispersion relations of electron density fluctuations in a Hall thruster plasma, observed by collective light scattering,” *Physics of Plasmas,* vol. 16, no. 3, Mar, 2009.

[13] J. Cavalier, N. Lemoine, G. Bonhomme *et al.*, “Hall thruster plasma fluctuations identified as the E x B electron drift instability: Modeling and fitting on experimental data,” *Physics of Plasmas,* vol. 20, no. 8, Aug, 2013.

[14] P. Coche, and L. Garrigues, “A two-dimensional (azimuthal-axial) particle-in-cell model of a Hall thruster,” *Physics of Plasmas,* vol. 21, no. 2, Feb, 2014.

[15] I. Katz, and I. G. Mikellides, “Neutral gas free molecular flow algorithm including ionization and walls for use in plasma simulations,” *Journal of Computational Physics,* vol. 230, no. 4, pp. 1454-1464, Feb 20, 2011.

[16] I. G. Mikellides, I. Katz, and R. R. Hofer, “Design of a Laboratory Hall Thruster with Magnetically Shielded Channel Walls, Phase I: Numerical Simulations,” in 47th AIAA/ASME/SAE/ASEE Joint Propulsion Conference, San Diego, CA, AIAA-2011-5809, July 2011, pp. 5809.

[17] I. G. Mikellides, I. Katz, R. R. Hofer *et al.*, “Design of a Laboratory Hall Thruster with Magnetically Shielded Channel Walls, Phase III: Comparison of Theory with Experiment,” in 48th AIAA/ASME/SAE/ASEE Joint Propulsion Conference, Atlanta, GA, AIAA-2012-3789, July 2012.

[18] A. L. Ortega, and I. G. Mikellides, “AIAA Paper No. 14-XXXX,” in Proceedings of the 50th AIAA Joint Propulsion Conference, Cleveland, OH, 2014, pp. XXXX.

[19] J. M. Haas, R. R. Hofer, D. L. Brown *et al.*, in 54th JANNAF Propulsion Meeting, Denver, CO, 2007.

[20] G. D. Hobbs, and J. A. Wesson, “Heat Flow through a Langmuir Sheath in Presence of Electron Emission,” *Plasma Physics,* vol. 9, no. 1, pp. 85-87, 1967.

[21] A. Harten, P. D. Lax, and B. Vanleer, “On Upstream Differencing and Godunov-Type Schemes for Hyperbolic Conservation-Laws,” *Siam Review,* vol. 25, no. 1, pp. 35-61, 1983.

[22] J. C. Butcher, “Numerical methods for ordinary differential equations in the 20th century,” *Journal of Computational and Applied Mathematics,* vol. 125, no. 1-2, pp. 1-29, Dec 15, 2000.

[23] I. G. Mikellides, I. Katz, R. R. Hofer *et al.*, “Magnetic Shielding of the Acceleration Channel Walls in a Long-Life Hall Thruster,” in 46th AIAA/ASME/SAE/ASEE Joint Propulsion Conference, Nashville, TN, AIAA-2010-6942, July 2010, pp. 6942.

[24] A. Lopez Ortega, and I. G. Mikellides, “The Importance of the Cathode Plume and its Interactions with the Ion Beam in Numerical Simulations of Hall thrusters,” in 34th International Electric Propulsion Conference, Hyogo-Kobe, Japan, IEPC-2015-310, July 2015.

[25] R. R. Hofer, I. Katz, I. G. Mikellides *et al.*, “Efficacy of Electron Mobility Models in Hybrid-PIC Hall Thruster Simulations,” in 44th AIAA/ASME/SAE/ASEE Joint Propulsion Conference, Hartford, CT, AIAA-2008-4924, July 2008.

[26] R. R. Hofer, D. M. Goebel, I. G. Mikellides *et al.*, “Magnetic shielding of a laboratory Hall thruster. II. Experiments,” *Journal of Applied Physics,* vol. 115, no. 4, Jan 28, 2014.

[27] W. Huang, and University of Michigan., "Study of Hall Thruster Discharge Channel Wall Erosion via Optical Diagnostics," 2011, p. 227 p.

[28] B. A. Jorns, R. R. Hofer, and D. M. Goebel, "Study of Probe Perturbation Effects in the H6US," Jet Propulsion Laboratory, California Institute of Technology, 2014, p. 52.

[29] B. A. Jorns, D. M. Goebel, and R. R. Hofer, “Plasma Perturbations in High-Speed Probing of Hall Thruster Discharge Chambers: Quantification and Mitigation ” in 51st AIAA/ASME/SAE/ASEE Joint Propulsion Conference, Orlando, FL, AIAA-2015-4006, July 2015.

[30] R. Z. Sagdeev, and A. Galeev, *Nonlinear plasma theory*, New York,: W. A. Benjamin, 1969.

[31] T. H. Stix, “Waves in Plasmas - Highlights from the Past and Present,” *Physics of Fluids B-Plasma Physics,* vol. 2, no. 8, pp. 1729-1743, Aug, 1990.

[32] N. A. Krall, and A. W. Trivelpiece, *Principles of plasma physics*, New York,: McGraw-Hill, 1973.

[33] I. Katz , A. Lopez Ortega , B. A. Jorns *et al.*, “Growth and Saturation of Ion Acoustic Waves in Hall Thrusters,” in 52nd AIAA/ASME/SAE/ASEE Joint Propulsion Conference, Salt Lake City, UT, AIAA-2016-XXXX, 2016.

[34] S. I. Braginskii, "Transport Processes in a Plasma," *Reviews of Plasma Physics*, M. A. Leontovich, ed., pp. 205-311, New York: Consultants Bureau, 1965.

[35] K. Appert, and J. Vaclavik, “Tail Formation by Non-Resonant Interaction of Ions with Ion-Acoustic Turbulence,” *Plasma Physics and Controlled Fusion*, vol. 23, no. 9, pp. 763-774, 1981.

[36] C. T. Dum, “Anomalous Heating by Ion Sound Turbulence,” *Physics of Fluids*, vol. 21, no. 6, pp. 945-955, 1978.

[37] C. T. Dum, R. Chodura, and D. Biskamp, “Turbulent Heating and Quenching of Ion Sound Instability,” *Physical Review Letters*, vol. 32, no. 22, pp. 1231-1234, 1974.

[38] C. A. Dodson, D. Perez-Grande, B. A. Jorns *et al.*, “Laser-induced Fluorescence Measurements of Energetic Ions in a 100-A LaB6 Hollow Cathode,” in 52nd AIAA/ASME/SAE/ASEE Joint Propulsion Conference, Salt Lake City, UT., AIAA-2016-XXXX, 2016., 2016.

[39] I. G. Mikellides, I. Katz, D. M. Goebel *et al.*, “Hollow cathode theory and experiment. II. A two-dimensional theoretical model of the emitter region,” *Journal of Applied Physics*, vol. 98, no. 11, Dec 1, 2005.

[40] I. G. Mikellides, I. Katz, D. A. Goebel *et al.*, “Wear mechanisms in electron sources for ion propulsion, 2: Discharge hollow cathode,” *Journal of Propulsion and Power*, vol. 24, no. 4, pp. 866-879, Jul-Aug, 2008.

[41] A. Lopez Ortega , I. G. Mikellides, and B. A. Jorns, “First-principles Modeling of IAT-driven Anomalous Resistivity in Hollow Cathode Discharges II: Numerical Simulations and Comparisons with Experiments,” in 52nd AIAA/ASME/SAE/ASEE Joint Propulsion Conference, Salt Lake City, UT., AIAA-2016-XXXX, 2016., 2016.

[42] B. A. Jorns, A. Lopez Ortega , and I. G. Mikellides, “First-principles Modeling of IAT-driven Anomalous Resistivity in Hollow Cathode Discharges I: Theory,” in 52nd AIAA/ASME/SAE/ASEE Joint Propulsion Conference, Salt Lake City, UT., AIAA-2016-XXXX, 2016, 2016.